Analytical Calculation of the Subthreshold Slope Increase in Short Channel MOSFET's by Taking the Drift Component into Account

Serge Biesemans, Kristin De Meyer

Advanced Silicon Devices Group
Interuniversity MicroElectronics Centre (IMEC),
Kapeldreef 75, B-3001 Leuven, Belgium

The subthreshold slope 'S' has been modelled based on the fundamental equations governing the behaviour of a MOSFET. By taking both, the diffusion as well as the drift component, into account, a physical complete description of the Short Channel effect on S has been accomplished. We calculate the potential from the Poisson, the minority carrier density from the continuity and the weak inversion current density from the drift-diffusion equation. This closed form expression for S accurately describes the gate length dependence.

1. Introduction

Attempts to model the subthreshold slope increase due to the Short Channel Effect (SCE) have scarcely been made [1]. All of them base their calculation of the subthreshold slope S on one hand on a non-constant surface potential in the lateral direction, typical for short channel FET's, but on the other hand use the expression for the subthreshold diffusion current. The contradiction in this scheme is that the diffusion current assumes a constant surface potential. We, on the contrary, calculate S based on a new short channel expression for the current, taking the drift (coming from the spatially dependent surface potential) as well as the diffusion component into account. This provides the means to model the short channel effect on S more consistent and physically founded. By writing the equations formally as a function of the 2D potential ψ, an extremely general description is obtained. 'General' in the sense that it is applicable to any device structure. We compare our calculations with 2D numerical simulation and experimental results.

2. The electron density

Take x as the lateral and y as the vertical coordinate. Within the Drift-Diffusion model, the x-component of the subthreshold current density for an nMOS is (but equally valid for pMOS after correct sign changes)

$$J_x = q\mu V_{th}\frac{\partial n}{\partial x} - q\mu n\frac{\partial \psi}{\partial x} \tag{1}$$

with n the free electron density, ψ the electrical potential and V_{th} the thermal voltage. A possible model for the electrical potential $\psi(x,y)$ in the channel is calculated elsewhere [2,3] and written as

$$\psi(x,y) = \psi^\circ(y) + (V_{bi} - \psi^\circ(y) + V_{DS})\left(\frac{\sinh(x/\lambda)}{\sinh(L/\lambda)}\right)$$
$$+ (V_{bi} - \psi^\circ(y))\left(\frac{\sinh((L-x)/\lambda)}{\sinh(L/\lambda)}\right) \tag{2}$$

with λ a natural length parameter depending on the particular device structure [3]. The y-dependence of the potential is taken to be parabolic, for instance in case of the planar bulk device $\psi^\circ(y)=\psi^\circ_s(1-y/t_{si})^2$ with ψ°_s the long channel surface potential at $V_{DS}=0$ V and t_{si} the depletion layer depth. Requiring the divergence of the current density J to be zero, we get following model for the electron density

$$V_{th}\frac{\partial^2 n}{\partial x^2} - \frac{\partial \psi}{\partial x}\frac{\partial n}{\partial x} - \frac{\partial^2 \psi}{\partial x^2}n = 0 \tag{3}$$

A possible solution of this equation is given by

$$n(x,y) = \exp\left(\frac{\psi(x,y) - \psi^\circ(y)}{V_{th}}\right)\left(N_1 + \right.$$
$$\left. N_2 \int_0^x \exp\left(-\frac{\psi(t,y) - \psi^\circ(y)}{V_{th}}\right)dt\right) \tag{4}$$

with N_1 and N_2 following from the two boundary conditions $n(0,y)=n(L,y)=N_{SD}$, the source and drain doping level. We plotted this function at the surface in Fig.1 for $V_{GS}=0$ V and $V_{DS}=0.5$ V, and compared it with the result of our 2D-device

simulator PRISM [4]. We observe that (4) follows well the trends of the numerical results.
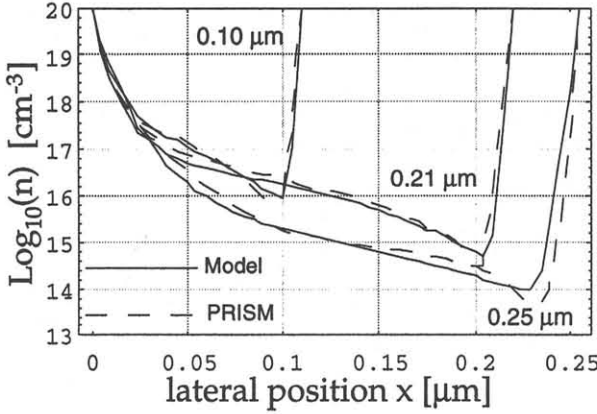
Fig.1 Surface free electron density in planar bulk device with $N_{sub}=10^{17}cm^{-3}$ and $t_{ox}=7nm$ for $L=0.25\mu m$ and $L=0.18\mu m$.

Even at the drain side, good agreement is obtained. By looking at (4), minor inaccuracies of ψ are exponentially magnified. But fortunately this turns out to be not a real problem for the current because an integration (which is a numerical smoothing process) is going to be carried out next.

3. The current density and the subthreshold slope

We calculated $\partial\psi/\partial x$ based on (2) and $\partial n/\partial x$ based on (4), plugged them into (1) and integrated it over the y-direction and the z-direction (the width of the device), resulting in

$$I = q\mu V_{th}n_i^2 N_{sub}^{-1}W\left(1-\exp\left(-\frac{V_{DS}}{V_{th}}\right)\right)\times$$

$$\int_0^\infty \frac{\exp\left(\frac{\psi^\circ(y)}{V_{th}}\right)}{\int_0^L \exp\left(-\frac{\psi(x,y)-\psi^\circ(y)}{V_{th}}\right)dx}dy \qquad (5)$$

In the limit for $L\to\infty$, $\psi(x,y)$ goes to the x-independent long channel value. In this case the integral in (5) reduces to the long channel subthreshold current expression (only the diffusion component) [5]. For the short channel case, the integral can easily be calculated numerically. We plotted in Fig.2 the simulated current (PRISM) and compared it against the long channel (1D) and the new 2D expression (5) for a Ground Plane device. We observe a much better agreement in the weak inversion regime for the new 2D expression.
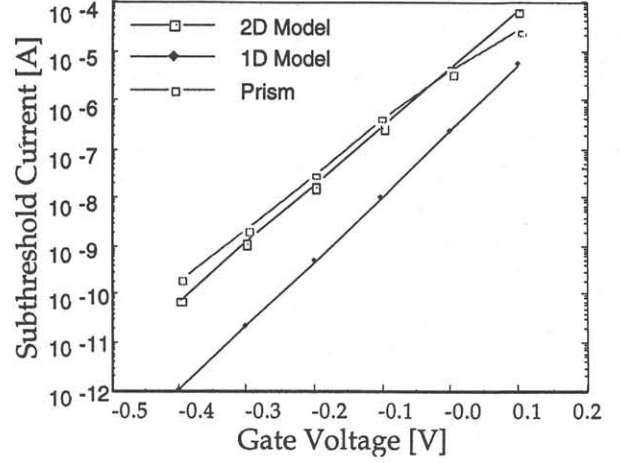
Fig.2 Subthreshold current in Ground Plane device with $L=0.1\mu m$, $t_{ox}=4nm$, $N_{surf}=10^{17}cm^{-3}$, $N_{bulk}=10^{18}cm^{-3}$, $t_{si}=50nm$, $V_{DS}=0.1V$ and $W=1\mu m$. Comparison with simulation result of PRISM.

Up to now, the analysis is general in that sense that it is device structural independent because all that information is hidden in λ. Examples of device structures are planar bulk, single gate SOI, double gate SOI, recessed bulk and the Ground plane. We proceed now by concentrating on the planar bulk device but the analysis can be applied as well to other structures as in Fig.2. Calculating $S=\ln(10)*\partial V_{GS}/\partial\psi_s*\partial\psi_s/\partial\ln(I)$, we get

$$S = \frac{kT}{q}Ln(10)\left(1+\frac{C_{Si}}{C_{ox}}\right)\left(\frac{1}{1-\frac{V_{th}}{2\psi_s^\circ}-\delta}\right) \qquad (6)$$

with

$$\delta = -\frac{V_{th}}{V_{bi}-\psi^\circ(0)}Ln\left(\frac{\int_0^L \exp\left(\frac{\psi^\circ(0)-\psi(x,0)}{V_{th}}\right)dx}{\int_0^L \exp\left(-\frac{V_{DS}}{V_{th}}\frac{\sinh(x/\lambda)}{\sinh(L/\lambda)}\right)dx}\right) \qquad (7)$$

We plotted in Fig.3 expression (6). In the limit for $\delta=0$, the long channel value of S is obtained which is independent of L. In general, for high N_{sub}, S increases because of the capacitor effect (third factor in (6)). In this region, only the diffusion component is important. Notice that the formula is independent of L. On the other hand, in the low N_{sub} region, the source/drain junction depletion regions extend further into the channel resulting in an increased drift component. This effect is taken into account by the δ. We plotted this in Fig.3 for two different
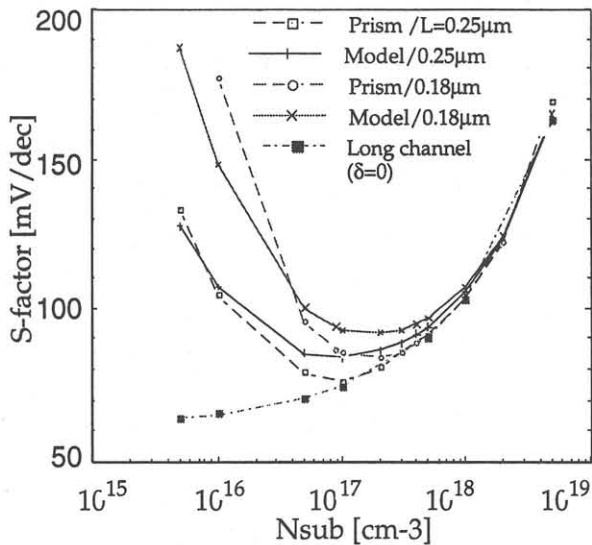
Fig.3 New 2D expression of S taking into account drift current for planar bulk device, t_{ox}=7.5nm, L=0.25μm and 0.18μm, V_{DS}=0.1V. Comparison between model (6) and 2D numerical simulation

Fig.4 Comparison of S (6) with experimental results from [6] for an SOI device, N_{sub}=3 10^{17}cm^{-3}, t_{ox}=7nm, t_{Box}=80nm, t_{si}=30nm, V_{DS}=0.1V

channel lengths using (7) and compared it with 2D numerical simulation. One observes now an L dependence in the low N_{sub} region and an increase of S due to the short channel effect.

Finally, we compared the model of S versus channel length for the SOI case with experimental results taken from literature [6], as shown in Fig.5. A very good agreement is obtained.

4. Conclusion

Through the calculation of the electron density and its spatial dependence, we were able to include the drift as well as the diffusion component in the expression for the subthreshold current. This resulted in a new formula for the S-factor, clearly showing the SCE coming in through the δ(drift)-parameter. In this way, the L-dependence of S could be included in a physically correct manner. In all cases, good agreement of the subthreshold current and subthreshold slope with simulation and/or experimental results is found.

5. References

[1]   H.O. Joachim, et al., IEEE TED, pp 1812-1817, 1993
[2]   Z.H. Liu, et al., IEEE TED, pp 86-93, 1993
[3]   S. Biesemans, et al., Workshop NUPAD V, Honolulu, 1994
[4]   R.C. Vankemmel, et al., IEEE Trans. on Computer Aided Design, pp 1786-1797, 1993
[5]   M. Shur, "Physics of semiconductor devices", Prentice Hall, pp 385-389, 1990
[6]   Y. Omura, IEICE TE, pp 1491-1497, Dec.'92